Acta Pharmaceutica Sinica B 2025;15(1):278−295

Chinese Pharmaceutical Association
Institute of Materia Medica, Chinese Academy of Medical Sciences

Acta Pharmaceutica Sinica B

www.elsevier.com/locate/apsb
www.sciencedirect.com

ORIGINAL ARTICLE

Dual activation of GCGR/GLP1R signaling ameliorates intestinal fibrosis *via* metabolic regulation of histone H3K9 lactylation in epithelial cells

Han Liu[a,b,†], Yujie Hong[a,†], Hui Chen[a,†], Xianggui Wang[a], Jiale Dong[a], Xiaoqian Li[a], Zihan Shi[a], Qian Zhao[a], Longyuan Zhou[c], JiaXin Wang[d], Qiuling Zeng[a], Qinglin Tang[a], Qi Liu[a], Florian Rieder[e], Baili Chen[c], Minhu Chen[c], Rui Wang[f,g], Yao Zhang[d,*], Ren Mao[c,*], Xianxing Jiang[a,*]

[a]*Guangdong Provincial Key Laboratory of Chiral Molecule and Drug Discovery, School of Pharmaceutical Sciences, Sun Yat-sen University, Guangzhou 510006, China*
[b]*State Key Laboratory for Animal Disease Control and Prevention, College of Veterinary Medicine, Lanzhou University, Lanzhou 730000, China*
[c]*Department of Gastroenterology, the First Affiliated Hospital of Sun Yat-sen University, Guangzhou 510080, China*
[d]*Department of Gastroenterology, Center for Immune-related Diseases, Ruijin Hospital, Shanghai Jiao Tong University School of Medicine, Shanghai 200025, China*
[e]*Department of Inflammation and Immunity, Lerner Research Institute, Cleveland Clinic Foundation, Cleveland, OH 44195, USA*
[f]*State Key Laboratory of Bioactive Substance and Function of Natural Medicines, Institute of Materia Medica, Chinese Academy of Medical Sciences & Peking Union Medical College, Beijing 100050, China*
[g]*School of Life Sciences, Key Laboratory of Preclinical Study for New Drugs of Gansu Province, School of Basic Medical Sciences & Research Unit of Peptide Science, Lanzhou University, Lanzhou 730000, China*

Received 11 April 2024; received in revised form 12 July 2024; accepted 26 July 2024

*Corresponding authors.
E-mail addresses: jiangxx5@mail.sysu.edu.cn (Xianxing Jiang), maor5@mail.sysu.edu.cn (Ren Mao), zyrjxh97@sjtu.edu.cn (Yao Zhang).
[†]These authors made equal contributions to this work.
Peer review under the responsibility of Chinese Pharmaceutical Association and Institute of Materia Medica, Chinese Academy of Medical Sciences.

https://doi.org/10.1016/j.apsb.2024.11.017

KEY WORDS

Glucagon receptor;
Glucagon-like peptide 1 receptor;
Lactate;
Glycolysis;
Post translational modification;
Epithelial-to-mesenchymal transition;
Intestinal fibrosis;
Peptide

Abstract Intestinal fibrosis is a significant clinical challenge in inflammatory bowel diseases, but no effective anti-fibrotic therapy is currently available. Glucagon receptor (GCGR) and glucagon-like peptide 1 receptor (GLP1R) are both peptide hormone receptors involved in energy metabolism of epithelial cells. However, their role in intestinal fibrosis and the underlying mechanisms remain largely unexplored. Herein GCGR and GLP1R were found to be reduced in the stenotic ileum of patients with Crohn's disease as well as in the fibrotic colon of mice with chronic colitis. The downregulation of GCGR and GLP1R led to the accumulation of the metabolic byproduct lactate, resulting in histone H3K9 lactylation and exacerbated intestinal fibrosis through epithelial-to-mesenchymal transition (EMT). Dual activating GCGR and GLP1R by peptide 1907B reduced the H3K9 lactylation in epithelial cells and ameliorated intestinal fibrosis *in vivo*. We uncovered the role of GCGR/GLP1R in regulating EMT involved in intestinal fibrosis *via* histone lactylation. Simultaneously activating GCGR/GLP1R with the novel dual agonist peptide 1907B holds promise as a treatment strategy for alleviating intestinal fibrosis.

1. Introduction

Intestinal fibrosis represents a challenge in treating inflammatory bowel disease (IBD), particularly in the case of Crohn's disease (CD)[1]. Fibrosis can lead to the development of intestinal fibrostenosis and even obstruction, requiring medical interventions[2]. The burden on patients and the lack of effective anti-fibrotic therapies have, in fact, motivated emerging studies to explore the underlying mechanisms driving intestinal fibrosis.

Like other fibrotic diseases, transforming growth factor β1 (TGFβ1) is a potent profibrotic mediator in the gut, playing a central role by inducing fibroblast proliferation and differentiation, promoting epithelial-to-mesenchymal transition (EMT), enhancing extracellular matrix (ECM) production and etc[3-5]. It triggers EMT, causing leading to extensive alterations in energy metabolism within the epithelial transcriptome, particularly in aerobic glycolysis[6,7]. As a primary byproduct of glycolysis, lactate has multiple biological functions but a number of these, including those involved in the regulation of intestinal fibrosis, remain unexplored. Recent studies suggest that lactate not only directly regulates protein functions[8-10], but also stimulates gene transcription through histone lactylation which modify lysine residues on histones[11-15]. This novel epigenetic modification holds important implications for cellular processes, including fibrosis. Indeed, lactate was found to increase histone lactylation in non-small cell lung cancer cells[16], challenging the conventional perspective of lactate as a mere metabolic byproduct and highlighting its potential as a therapeutic target for fibrotic disorders[17-19].

Glucagon receptor (GCGR) and glucagon-like peptide 1 receptor (GLP1R) are both peptide hormone receptors closely related to glycometabolism[20,21]. Previous studies have emphasized their dual action, which can impact key metabolic and pathological components of non-alcoholic steatohepatitis, in part by mitigating fibrosis[22-24]. Indeed, GLP1R is predominantly expressed in epithelial cells, with reduced mRNA levels observed in the colon of both ulcerative colitis and CD patients[25]. GLP1R signaling is linked to a novel axis that regulates innate immunity, gut barrier function, epithelial turnover, and the host response to enteric pathogens in intestinal intraepithelial lymphocytes[26]. Enhancing GLP1R signaling could also promote intestinotrophic activity in *Gcgr*$^{-/-}$ mice, either in the small bowel or colon, hence indicating synergistic action[27]. This elegant work suggested that the simultaneous targeting of GCGR and GLP1R could be a promising therapeutic strategy in the treatment of intestinal fibrosis, especially its novel metabolism-related mechanism.

In this study, we ultimately revealed a positive feedback loop consisting of decreased GCGR/GLP1R expression, lactate accumulation and histone H3K9 lactylation (H3K9la). In addition, it was shown how this loop could exacerbate EMT in intestinal fibrosis (Fig. 1A). Based on both pharmacological and genetic approaches, a GCGR/GLP1R co-agonist peptide (1907B) were also determined to inhibit the development of intestinal fibrosis according to this loop. Overall, this study revealed that the GCGR/GLP1R−lactate axis could be a novel therapeutic target for intestinal fibrosis associated with IBD.

2. Materials and methods

2.1. Synthesis of peptides

A series of GCGR/GLP1R dual-target peptides were synthesized using the standard protocol of solid-phase peptide synthesis on 4-methylbenzhydrylamine resin (GL Biochem, Shanghai, China). The synthesis was manually performed on a chemical rotary shaker (SYNTHWARE, Beijing, China). Reversed-phase high-performance liquid chromatography-mass spectrometric (RP-HPLC−MS, Agilent Technologies, USA) was used to perform the peptide purification and atomic accumulation process. All peptides were processed to >95% purity, and their peptide sequence identity was confirmed by mass spectrometry. The excitation activity data of the GCGR/GLP1R dual-target peptides are listed in Supporting Information Table S1.

2.2. Procurement and histopathology of intestinal tissues

Freshly resected intestinal specimens (full thickness) were obtained from subjects with CD as previously described, alongside controls comprised healthy tissues (healthy margin of resections from colorectal cancer patients; termed NL for normal)[28]. The CD specimens were then classified, based on gross anatomy, into strictured (CD-S) and non-strictured (CD-NS) samples. Our procurement system was validated by a trained IBD pathologist

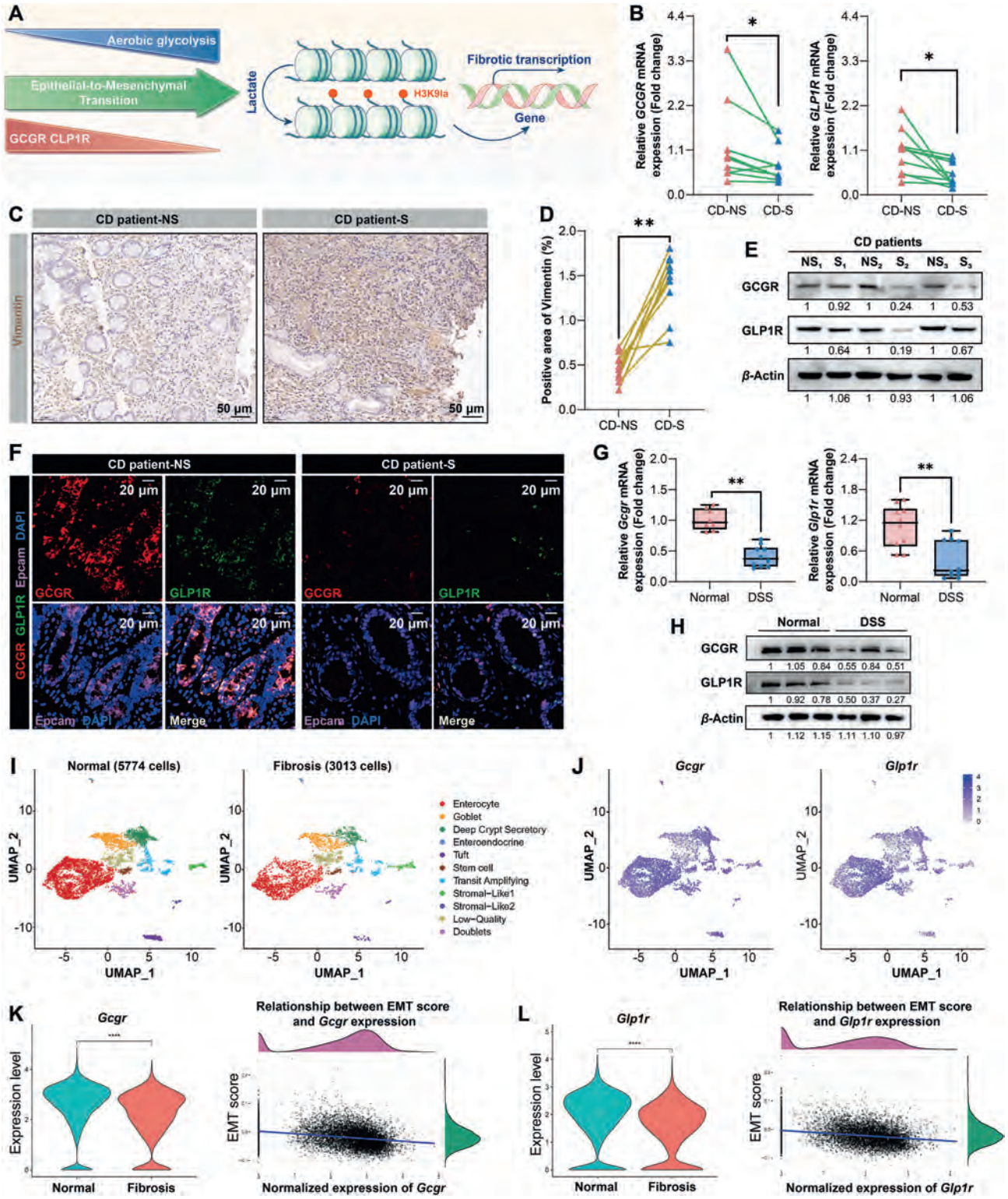

Figure 1 Expression of GCGR and GLP1R is correlated with EMT in intestinal fibrosis. (A) The scheme of the GCGR/GLP1R−lactate axis in intestinal fibrosis. (B) The expression of *GCGR* and *GLP1R* mRNA in CD patients' intestine ($n = 10$ patients). The data is presented as symbol and lines. (C, D) Representative immunohistochemical staining and semiquantitative image analysis of Vimentin in the intestine from CD patients ($n = 10$ patients). (E) Representative Western blot images of GCGR and GLP1R in CD patients' intestine ($n = 3$ patients). (F) Representative *in situ* hybridization images of *GCGR* and *GLP1R* mRNA expression in the intestine from CD patients ($n = 10$ patients). (G) Expression of *Gcgr* and *Glp1r* mRNA in intestine from mice ($n = 8-10$). The data is presented as min to max using box plot. (H) Representative Western blot images of GCGR and GLP1R protein in intestine from mice ($n = 3$). (I) Uniform manifold approximation and projection (UMAP) plots from control and experimental chronic colonic fibrosis mice. (J) Feature plots showing the expression distribution of *Gcgr* and *Glp1r* in intestinal epithelial cells. (K, L) Violin plots and scatter plots in intestinal epithelial cells between control and experimental chronic colonic fibrosis mice. $^*P < 0.05$, $^{**}P < 0.01$ *vs* as indicated.

(IOG) through histopathologic evaluation. Molecular characterizations, including immunohistochemistry, Western blot and quantitative real-time polymerase chain reaction (qRT-PCR), were subsequently performed. All clinical Intestinal samples were obtained from the First Affiliated Hospitals of Sun Yat-sen University (Guangzhou, China). All procedures were performed in compliance with relevant laws and institutional guidelines. The study was approved by the institutional ethics review board of the First Affiliated Hospital, Sun Yat-sen University [No. (2023)113]. Informed consents were signed by patients with CD. The information on patients is listed in Supporting Information Table S2.

2.3. Animals

Male C57BL/6J and BALB/c mice, aged 6−8 weeks old, were obtained from the Guangdong Medical Laboratory Animal Center (certificate No. SCXK 2022-0002). Mice in groups of 4−6 animals per cage were housed with a 12 h light/dark cycle lighting schedule and were given free access to food and water at a temperature of 24.0 ± 0.5 °C. The time for experimentation was from 09:30 am to 11:30 am and the testing order was randomized daily, with each animal tested at a different time each test day. All experiments were approved by the Ethics Committee on Use and Care of Animals of Sun Yat-sen University (SYSU-IACUC-2023-000631), and the instructions of Guide for Care and Use of Laboratory Animals from NIH. The applicable Bolder BioPATH standard operating procedures were strictly followed for all treatments and handling of animals. All efforts were made to minimize animal suffering and reduce the number of animals used.

2.4. Induction of chronic colitis in mice

To induce chronic colitis-associated colonic fibrosis, mice received 2% dextran sulfate sodium (DSS) or 2.5% trinitro-benzene-sulfonic acid (TNBS)[29]. (1) For the 2%DSS-induced chronic model, mice received 2%DSS in the drinking water for 1 week, followed by 2 weeks of normal drinking water. This cycle was repeated 3 times. Mice were randomized and treated 240 μg/kg 1907B subcutaneously every other day after the second cycle of DSS (n = 10 mice per group, a total of 30 mice). Mice were divided into three groups: Normal (control), 2%DSS (model) and 2%DSS+1907B. (2) For 2.5% 2,4,6-trinitrobenzenesulphonic acid (TNBS; Sigma, Shanghai, China)-induced chronic model, BALB/c mice were anesthetized by isoflurane (0.41 mL/min at 4 L/min fresh gas flow, working concentration: 2%), and 0.1 mL of 50% ethanol (vehicle), or TNBS (50 mg/kg) dissolved in 50% ethanol were administered into the colon through a rubber catheter. The experiment was repeated weekly for 6 weeks. Mice were randomized and subcutaneously treated with 240 μg/kg 1907B every other day after the fourth week (n = 3 mice per group, a total of 9 mice). Mice were divided into three groups: Vehicle (control), TNBS (model), and TNBS+1907B.

For each animal, three different investigators were involved as follows: the first investigator was responsible for model induction, the second investigator administered the treatment, and was the only person aware of the treatment group allocation, finally, the third investigator (also unaware of treatment) assessed and recorded the fecal state.

Mice were monitored daily for stool consistency and hematochezia. Mice were randomized based on their rectal bleeding and diarrhea scores. The score of stool blood (score = 0: absence, 2: presence, 4: gross bleeding) and stool consistency (score = 0: formed and hard, 1: formed but soft, 2: loose stools, 3: mild diarrhea, 4: gross diarrhea) were recorded[29]. Haemoccult test (Baso, Zhuhai, China) was used to measure the presence of blood in the stool. The mice were sacrificed to analyze the serum and colon tissue.

2.5. Adeno-associated virus 9 (AAV9)-RNAi-mediated Glp1r and Gcgr knockdown

The AAV9 carrying shRNA for mouse *Glp1r* (AAV9-*Glp1r*-shRNA), shRNA for mouse *Gcgr* (AAV9-*Gcgr*-shRNA), and mouse nonsense control shRNA (AAV9-NC-shRNA) were custom-made from Genechem (Shanghai, China). The administration procedures were performed according to previous studies[30]. The adeno-associated virus was injected into mice (10^{11} v.g., *via* tail vein) to knock down *Glp1r* and *Gcgr*. The target sequences used for knockdown are listed in Supporting Information Table S3.

Animals were randomized using a computer-based random order generator. After 3 weeks of injection with AAV9-RNAi to knock down *Glp1r* and *Gcgr*, C57BL/6J mice were used to establish the DSS-induced chronic model, as above described. Mice were classified into three groups: shNC group (rats injected with AAV9-NC-shRNA), 2%DSS+shNC group (rats administered with 2%DSS solution and injected with AAV9-NC-shRNA) and 2%DSS+sh*Gcgr*-sh*Glp1r* group (rats administered with 2%DSS solution and injected with AAV9-*Glp1r*-shRNA and AAV9-*Gcgr*-shRNA). The mice were sacrificed to harvest the colon tissue (n = 6 mice per group, a total of 18 mice) for metabolomic analysis and Masson staining. The degree of colon fibrosis was evaluated by a semi-quantitative analysis in the blue-dyed region of Masson microscopic images.

2.6. Isolation of primary mouse colon epithelial cells in vitro

As described in the previous study with some modifications[31], colons obtained from mice were cut into small pieces, washed, and then digested at 37 °C on a shaking platform at 60 rpm for 20 min. After shaking and mixing, the digestive fluid containing the intestinal segments was filtered through a 100 μm cell strainer, the first filtrate was collected, and placed on ice. The intestinal segments were transferred to a centrifuge tube containing digestive fluid and incubated at 37 °C on a shaking platform at 60 rpm for 20 min. After shaking and mixing, the digestive fluid containing the intestinal segments was filtered through a 100 μm cell strainer. The collected filtrate was combined with the first filtrate and added phosphate buffered saline (PBS) buffer to a final volume of 35 mL. After centrifuging at 250×g for 10 min at 4 °C, the resulting pellet was the isolated epithelial cells. Epithelial digestive fluid: HBSS balanced salt solution (without calcium and magnesium, with phenol red) 288 mL, 2% fetal bovine serum 6 mL, 5 mmol/L EDTA Na_2 332 mL, 2 mmol/L DTT 300 mL, 100 × HEPES solution 3 mL, 100 × penicillin−streptomycin antibiotic mixture 3 mL.

2.7. Morphology and histology

The mice were euthanized, the colon was removed, and its length and weight were recorded. The colon tissue was then fixed in 10% neutral buffered formalin and embedded in paraffin. Histological sections of 5 μm were prepared and stained with hematoxylin-eosin and Masson. Images of the tissue sections were digitally acquired, and morphometric analyses were performed.

2.8. *In situ hybridization*

In situ hybridization was performed on clinical and mouse tissue samples embedded in 4 μm-thick paraffin to detect the expression of *GCGR* (or *Gcgr*) and *GLP1R* (or *Glp1r*) mRNA. Samples were fixed, sectioned, and hybridized with the probes specific for each target gene (Servicebio, Wuhan, China). The sequences of probes used are listed in Supporting Information Table S4. Slices were observed and images were captured using an upright fluorescence microscope (3DHISTECH, Budapest, Hungary).

2.9. *Luminex assay*

The whole blood was centrifuged at 1600 × *g* for 10 min at 4 °C to obtain serum samples. The cytokines present in the serum were analyzed using a mouse magnetic Luminex assay (R&D system, CA, USA) with the help of a Luminex 200™ instrument (Luminex Corporation, TX, USA).

2.10. *Metabolomic analysis of mice colon*

Mice were infected with AAV9 to knockdown *Glp1r* and *Gcgr*, and then used in the DSS-induced chronic model, with their colon subsequently pretreated by following corresponding protocol[32,33]. All those metabolites were detected by MetWare (http://www.metware.cn/) based on the AB Sciex QTRAP 6500 LC−MS/MS platform (Wuhan, China). The metabolites with fold change $\geq$1.2 or fold change $\leq$0.67 were considered significant.

2.11. *Tissue dissociation and single-cell RNA sequencing (scRNA-seq) of mouse colon*

Following the removal of adipose tissue and visible blood vessels, colons from C57BL/6J mice were treated with water and chronic 2% DSS (n = 3), and were collected. Subsequently, they were washed with ice-cold PBS and cut into small approximately 0.25 cm-long fragments. These tissue fragments were then digested in 1640 medium supplemented with 10% fetal bovine serum, collagenase type VIII (50 U/mL), and DNase I (50 U/mL) at 37 °C for 60 min. After digestion, the remaining tissue fragments were collected into a 15 mL tube, vortexed vigorously for 30 s, and mechanically dissociated using 21-gauge syringes. The resulting cell suspension was filtered through a 70 μm cell strainer. The obtained cell suspension was centrifuged at 350 × *g* and 4 °C for 5 min. The supernatant was discarded, and the cells were resuspended in single-cell buffer (PBS supplemented with 10% fetal bovine serum) for single-cell RNA sequencing. The single-cell suspensions were processed using the Chromium Next GEM Single Cell 5′ Kit v2 (10 × Genomics) following the manufacturer's instructions. The libraries were sequenced using the Illumina HiSeq X-Ten sequencer.

2.12. *Analysis of single-cell RNA-seq data*

The sequencing data were processed using Cell Ranger software (10 × Genomics). The reads were mapped to the mouse reference genome (mm10) using Cell Ranger v5.0.1. The resulting preliminary count matrices were further analyzed using the R package Seurat v4.1.1. Cells with unique molecular identifier (UMI) counts ranging from 500 to 50,000 and detected genes ranging from 200 to 6000 and cells that contained less than 25% mitochondrial gene counts were retained. To identify potential doublets, we used the Python packages Scrublet v0.2.3 and DoubletDetection v4.2 with default parameters. Following quality control, a total of 53,817 cells from the mouse model samples finally remained. Normalization, log scale, dimension reduction, and unsupervised clustering were performed using the standard workflow in Seurat. After the initial round of unsupervised clustering, major cell types were annotated including epithelial cells, myeloid cells, T/NK cells, B/plasma cells, endothelial cells, and stromal cells based on known canonical cell markers. Subsequently, a total of 8787 epithelial cells were subject to a second round of unsupervised clustering to identify distinct cell subsets. To correct for batch effects, the Harmony algorithm from the R package Harmony v1.0 was utilized. Cell cluster-specific marker genes were identified using the FindAllMarkers function in Seurat. Next, the expression levels of *Gcgr/Glp1r* were compared between the two groups, and the non-parametric Wilcoxon rank-sum test was used to obtain P value for comparisons. The gene set (GO:0001837) was downloaded from MSigDB, and the AddModuleScore function in Seurat was used to calculate the EMT score. Pearson correlation analysis was performed to assess the relationship between normalized *Gcgr/Glp1r* expression and the EMT score in epithelial cells.

2.13. *Cell culture and treatment*

Rat normal intestinal crypt epithelial cell line IEC-6 and human colon cancer cell line SW480 were provided by Procell (Wuhan, China). The IEC6 cells and SW480 cells were cultured in high-glucose Dulbecco's modified Eagle's medium (DMEM; Gibco, CA, USA) and leibovitz's L-15 medium (Servicebio, Wuhan, China), respectively, supplemented with 10% heat-inactivated fetal calf serum and 1% penicillin−streptomycin. IEC6 cells were incubated under 37 °C and 5% CO_2 conditions, while SW480 cells were incubated under 100% air (CO_2-free) conditions and cultured with 2 mmol L-glutamine (Servicebio, Wuhan, China). When IEC6 cells reached 40% sub-confluency, the medium was replaced with serum-free medium for at least 6 h before adding 10 ng/mL TGFβ1 (Novoprotein, Suzhou, China) for 3 or 7 days, and medium was changed every two days. The cells were then harvested, and the expression of specified protein and RNA was studied as indicated.

2.14. *RNAi transfection*

The lentivirus carrying shRNA for rat *Glp-1r* and *Gcgr* were provided by ObiO (Shanghai, China). The stable cells with knockdown of *Glp1r* or *Gcgr* were selected and amplified using with a real-time dynamic live cell imaging high-content system (IncuCyte ZOOM, Essen Bioscience, MI, USA). The clones were verified by qRT-PCR and Western blotting. The stable IEC6-shRNA *Glp1r* $1^{\#}$ and *Gcgr* $1^{\#}$ cells were selected. The interference vector was pSLenti-U6-shRNA-CMV-EGFP-F2A-Puro-WPRE. Corresponding plasmid information is listed in Supporting Information Table S5.

The mutated H2B (K16R), H3.1 (K9R), and H4 (K5R) overexpressing vector was developed using eukaryotic vector pCDNA3.1-CMV-MCS-hGHpolya-EF1a-EGFP (ObiO, Shanghai, China). Corresponding plasmid information is listed in the session "Plasmid sequence of histone overexpression" of Supporting Information (Materials).

2.15. Seahorse XF real-time ATP rate assay

For the real-time ATP rate analysis, the indicated IEC6 cells were plated onto the Seahorse XFe96 cell culture microplates (Agilent, Palo Alto, CA, USA). Cells were treated with TGFβ1 and/or 1907B for 7 days. The medium was then replaced with Seahorse XF DMEM, pH 7.4 supplemented with 10 mmol glucose, 2 mmol glutamine, and 1 mmol pyruvate and incubated in a non-CO_2 incubator for 1 h at 37 °C prior to the start of the assay. Afterwards, basal levels of oxygen consumption rate (OCR) and extracellular acidification rate (ECAR) were then recorded. ATP production rate was measured using 1.5 μmol oligomycin and 0.5 μmol rotenone/antimycin A according to the manufacturer's instructions. OCR and ECAR data were normalized to the protein content as assessed by BCA assay.

2.16. Lactate determination

Frozen human intestinal specimens, mice colon, and cultured cells were homogenized with lysis buffer, and cell culture supernatant were collected immediately. The concentrations of lactate were measured using CheKine™ Lactate Assay Kit (Abbkine, Wuhan, China) according to manufacturer's instructions.

2.17. Fluorescent immunohistochemistry and immunocytochemistry

After fixing, permeabilization and blocking, sections or cells were incubated with primary antibodies overnight at 4 °C. Then, slides were incubated with goat anti-mouse/rabbit IgG secondary antibodies for 1 h. Coverslips were mounted with antifade mounting medium (Solarbio, Beijing, China) and fluorescence was observed under a fluorescence microscope (FV3000, Olympus, Tokyo, Japan). The antibodies used are listed in Supporting Information Table S6.

2.18. Histone exaction

The histones were extracted using the acid precipitation method[34]. For nuclei extraction, cells were collected and resuspended in lysis buffer containing protease inhibitors. Nuclei were then resuspended in 0.2 mol/L H_2SO_4 and extracted overnight at 4 °C followed by centrifugation at 16,000 × g for 10 min at 4 °C. The supernatant was collected, and the histone pellet was precipitated with 35% trichloroacetic acid on ice. The histone pellet was washed with acetone, dissolved in H_2O, and subjected to protein concentration measurement using the BCA assay (Thermo Fisher, MA, USA) prepared for Western blotting analysis.

2.19. Measurement of lysine lactylation

For total protein, lysine lactylation levels were detected using lactylation pan-antibody (PTM BIO, Hangzhou, China), and displayed by the uncropped gels. For histones, cells were collected and then the histones were extracted using the acid precipitation method[34]. Primary antibodies were used to detect the lysine lactylation modification levels at specific sites of the histones. For this experiment, a deacetylase inhibitor cocktail (Beyotime, Shanghai, China) was added to all lysates. The antibodies used are listed in Table S6.

2.20. Western botting

Tissues or cells were lysed in a lysis buffer and quantified by the BCA method. Protein concentration in the supernatants was determined with a protein assay kit. Total protein or histone was separated by sodium dodecyl sulphate-polyacrylamide gel electrophoresis gel system and transferred to a 0.22 μm polyvinylidene fluoride membrane (Millipore Corp, MA, USA). The blot was incubated overnight with primary antibodies at 4 °C. Afterwards, corresponding peroxidase-conjugated affinipure anti-goat anti-mouse or anti-rabbit IgG(H+L) antibody was added. Blots were visualized using ECL reagent (New Cell & Molecular Biotech, Suzhou, China) and scanned by a chemiluminescence-detection apparatus (Clinx, Shanghai, China). The primary antibodies are shown in Table S6.

2.21. qRT-PCR

RNA was extracted from human and C57BL/6J mice tissue or cells following the manufacturer's guidelines. Particularly, prior to extraction, mouse intestinal RNA was purified using the lithium chloride method due to the potent inhibition of qRT-PCR amplification of mRNA caused by DSS contamination. Then RNA was reversed transcribed into cDNA using the reverse transcription kit (Vazyme, Nanjing, China). The qRT-PCR analysis was performed using a qPCR kit (Vazyme, Nanjing, China) on a real-time PCR amplifier (Roche, Basel, Switzerland). Primer sequences are listed in Supporting Information Tables S7−S9. Relative gene expression was determined as Eq. (1):

$$\text{Change in expression (fold)} = 2^{-\Delta(\Delta CT)} \quad (1)$$

where ΔCT = CT (target)−CT (housekeeping), and $\Delta(\Delta CT)$ = ΔCT (treated)−ΔCT (control). The housekeeping gene, β-actin was used as the control.

2.22. Chromatin immunoprecipitation (ChIP) assay

Native chromatin IP assays were performed as manufacturer's instructions (Active Motif, CA, USA). Briefly, cells were collected in lysis buffer, then genomic DNA was sheared using enzyme to lengths of approximately 100−600 bp. IP was performed using anti-lactyl-lysine antibody (PTM-1419; PTM Biolabs, Hangzhou, China) and protein G. Genomic DNA in the immunocomplexes was purified using the phenol-chloroform method. Primer sequences to amplify the promoter regions of rat genes were listed in Supporting Information Table S10.

2.23. Quantification and statistical analysis

The area with positively stained slices was quantified by Image-Pro Plus, and the relative band density of Western blot was analyzed by ImageJ. GraphPad Prism 9.0 software was used to determine the statistical significance. Statistical significance was calculated by Student's t-test between two groups or one-way ANOVA followed by Dunnett's multiple comparisons test more than two groups. Significance was considered when $^{*}P < 0.05$ or $^{**}P < 0.01$.

3. Results

3.1. Decreased expression of GCGR and GLP1R in the fibrotic intestines of CD

In this study, a decrease in the mRNA and protein levels of GCGR/GLP1R was first observed in the stenotic intestine of patients with CD (Fig. 1B and E) as well as in the fibrotic colon of mice with chronic colitis (Fig. 1G and H, Supporting Information Fig. S1A).

In situ hybridization analysis further found that *GCGR* and *GLP1R* were widely expressed in the non-strictured sites of the CD patients' intestine (Fig. 1F), while their expression was downregulated in strictured ones, particularly in the human intestinal epithelium (Fig. 1F). Therefore, it was speculated that the downregulation of GCGR and GLP1R could be associated with EMT, as epithelial cells undergo EMT to promote intestinal fibrosis. Further immunohistochemistry analysis revealed an upregulation of the EMT marker Vimentin in the strictured sites (Fig. 1C and D), contrary to the trend observed for GCGR and GLP1R.

Colon scRNA-seq of C57BL6J mice was performed to confirm the relationship between GCGR/GLP1R expression and EMT. Eleven distinct intestinal epithelial subclusters of mice (Fig. 1I, Fig. S1B and S1C) were identified by scRNA-seq, revealing a decrease in *Gcgr*/*Glp1r* expression in these cells (Fig. 1J−L). Furthermore, scRNA-seq demonstrated a significant negative correlation between EMT scores and the *Gcgr*/*Glp1r* expression of the epithelial cells (Fig. 1K and L), which was in accordance with the immunohistochemical staining of Vimentin in CD patients (Fig. 1C and D).

Collectively, the downregulation of GCGR/GLP1R in epithelial cells, along with the negative correlation with EMT, suggests that GCGR/GLP1R may be involved in fibrosis by influencing EMT.

3.2. Knockdown of GCGR and GLP1R increases intestinal glycolysis metabolites of lactate and aggravates intestinal fibrosis

Recombinant AAV9-mediated gene delivery to intestinal epithelial cells provides a new strategy of gut transduction and allows the study of intestinal diseases[35]. Our group has successfully applied and consistently employed AAV9-mediated gene knockdown strategies across multiple animal models[23,36]. According to the previous study, AAV9, which provides relatively high efficiency in gut transduction[37], was selected to transfect mice with AAV9-*Glp1r*-shRNA and AAV9-*Gcgr*-shRNA or AAV9-NC-shRNA through tail vein injection. To determine intestinal efficiency *in vivo*, preliminary experiment and the following qRT-PCR assay were used to detect gene expression in colons (Supporting Information Fig. S2A−S2C).

Firstly, we used the AAV9-mediated genetic approaches combined with 2% DSS-induced chronic model to determine whether the downregulation of GCGR and GLP1R affects the phenotype of intestinal fibrosis (Fig. 2A). In the chronic model, Masson staining revealed that *Gcgr*/*Glp1r* dual knockdown worsened the degree of fibrosis in mice (Fig. 2B and C), as well as COL1A1 immunohistochemical staining (Fig. S2F and S2G). Colon length and HE staining were seen in Fig. S2D, S2E and S2G. These findings further proved the significant role of GLP1R and GCGR in intestinal fibrosis.

Due to their role as metabolism-related receptors, an energy metabonomic analysis was undertaken on colon tissues of chronic DSS-injured mice to explore the potential mechanism. The principal component analysis was first carried out to detect intrinsic clustering between groups (Fig. S2H). Overall, the results revealed that after downregulation of GCGR and GLP1R, the significant changes were observed in glycolysis-related metabolites (Fig. 2E), with lactate exhibiting the most prominent alterations (Fig. 2F). In particular, 26 compounds were significantly different between the 2% DSS-induced intestinal chronic colitis group and shNC group, and divided into the following four classes, starting with the most significantly different metabolite: glycolysis, pentose phosphate pathway, the citric acid cycle (TCA), and oxidative phosphorylation (OXPHOS) (Fig. 2D). The metabolites were then quantified in DSS-injured mice treated with AAV9-*Gcgr*-*Glp1r* shRNA. Compared with the 2% DSS + shNC group, 21 compounds were classified as being from the pentose phosphate pathway, glycolysis and TCA cycle (Fig. 2E). Glycolysis was the subject of focus because of its maximum proportion in chronic colitis, and those glycolytic metabolites for which the levels had also changed in knockdown mice were marked with a light pink column (Fig. 2D and E). Levels of these glycolysis metabolites, including glycerol-3-phosphate, 3-phosphoglycerate, pyruvic acid, lactate (Fig. 2F) and others (Fig. S2I) were also displayed. Of the several glycolytic byproducts, lactate was found to change dramatically as a result of *Gcgr* and *Glp1r* knockdown (Fig. 2F).

Lactate levels were notably higher in strictured sites compared with non-strictured ones in the CD patients' intestines (Fig. 2G), hence suggesting a possible association between lactate concentrations and fibrosis. To verify the relationship between GCGR/GLP1R expression and lactate, correlation analyses were conducted in DSS-injured mice. Accordingly, the mRNA levels of GLP1R and GCGR were found to be negatively correlated with lactate level in the intestine (Fig. 2H). These results collectively indicated that a deficiency in *Glp1r* and *Gcgr* could induce intestinal fibrosis, with the underlying mechanism may involve metabolism, especially the upregulation of glycolysis product lactate.

3.3. Lactate promotes EMT-mediated intestinal fibrosis in epithelial cells

To ascertain whether the regulatory processes of GCGR and GLP1R on lactate also exist at the cellular level, IEC6 cells were used to establish an intestinal EMT cell model (Supporting Information Fig. S3A). Consistent with the aforementioned *in vivo* observations, the results from the cell model revealed that during the EMT process, changes occurred in the expression of metabolism-related genes (Supporting Information Figs. S3B, S3E, S4A, S4B, and S4C), leading to an accelerated glycolytic rate (Fig. 3A, Fig. S3C and S3D). This, in turn, contributed to the production of lactate (Fig. 3C), as well as the change of serine−glycine biosynthetic pathway and gluconeogenesis (Fig. S3F, S3G, and S3H).

To investigate the impact of inhibiting glycolysis on EMT, we utilized inhibitors to separately target glycolysis and lactate production. 2-Deoxy-D-glucose (2DG), a glucose analogue, effectively inhibited glycolysis (Fig. 3B), leading to a substantial reduction in lactate levels (Fig. 3C) as well as the expression of fibrotic genes and proteins (Fig. 3D and Fig. S4D). The GSEA-KEGG plot between TGFβ1+2DG group and TGFβ1 group showed changes in metabolism-related genes, particularly in glycolysis-associated genes which displayed the largest number of genes being downregulated following 2DG treatment (Fig. 3E and Fig. S4B).

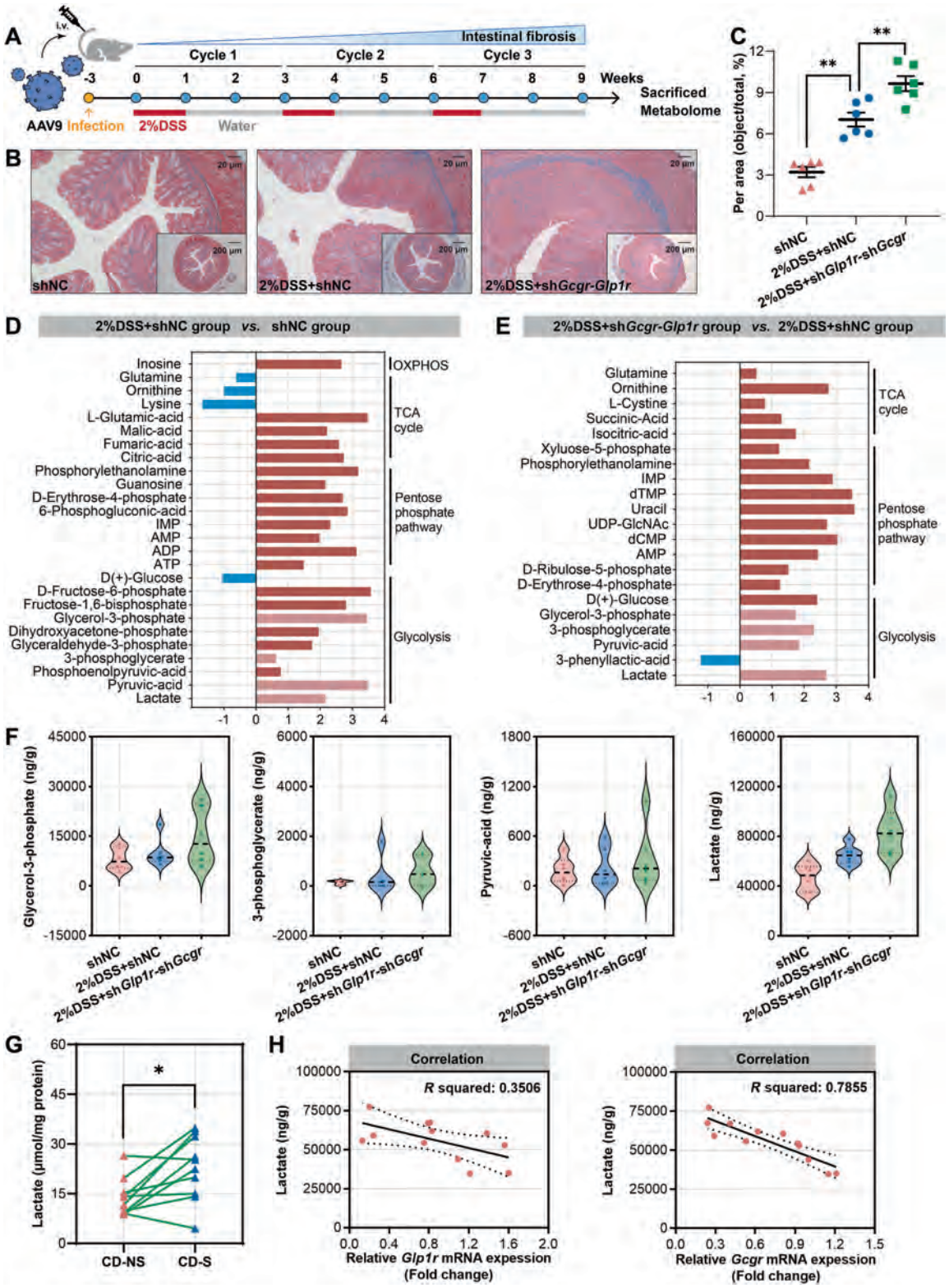

Figure 2 GCGR and GLP1R downregulation regulates metabolic reprogramming in intestinal fibrosis. (A) Schematic experimental workflow of *in vivo* DSS-induced chronic colitis and AAV9-mediated *Gcgr* and *Glp1r* knockdown. (B) Representative images of Masson staining ($n = 6$). (C) Semiquantitative image analysis of Masson staining ($n = 6$). The data is presented as mean ± SEM. (D) Energy metabonomic analysis was conducted on colon tissue between the 2%DSS + shNC group and shNC group ($n = 6$). (E) Energy metabonomic analysis was conducted on colon tissue between the 2% DSS + AAV9-*Glp1r-Gcgr* group and the 2%DSS + shNC group ($n = 6$). (F) The levels of typical differential glycolytic metabolites in each group ($n = 6$). The data are presented using violin plot. (G) The levels of lactate ($n = 10$ patients) in the intestine from CD patients at the normal site (CD-NS), stenosis site (CD-S). The data is presented as symbol and lines. (H) Correlation between GCGR/GLP-1R expression and lactate level on colon tissue from chronically DSS-injured mice ($n = 12$). $^{**}P < 0.01$ *vs* as indicated.

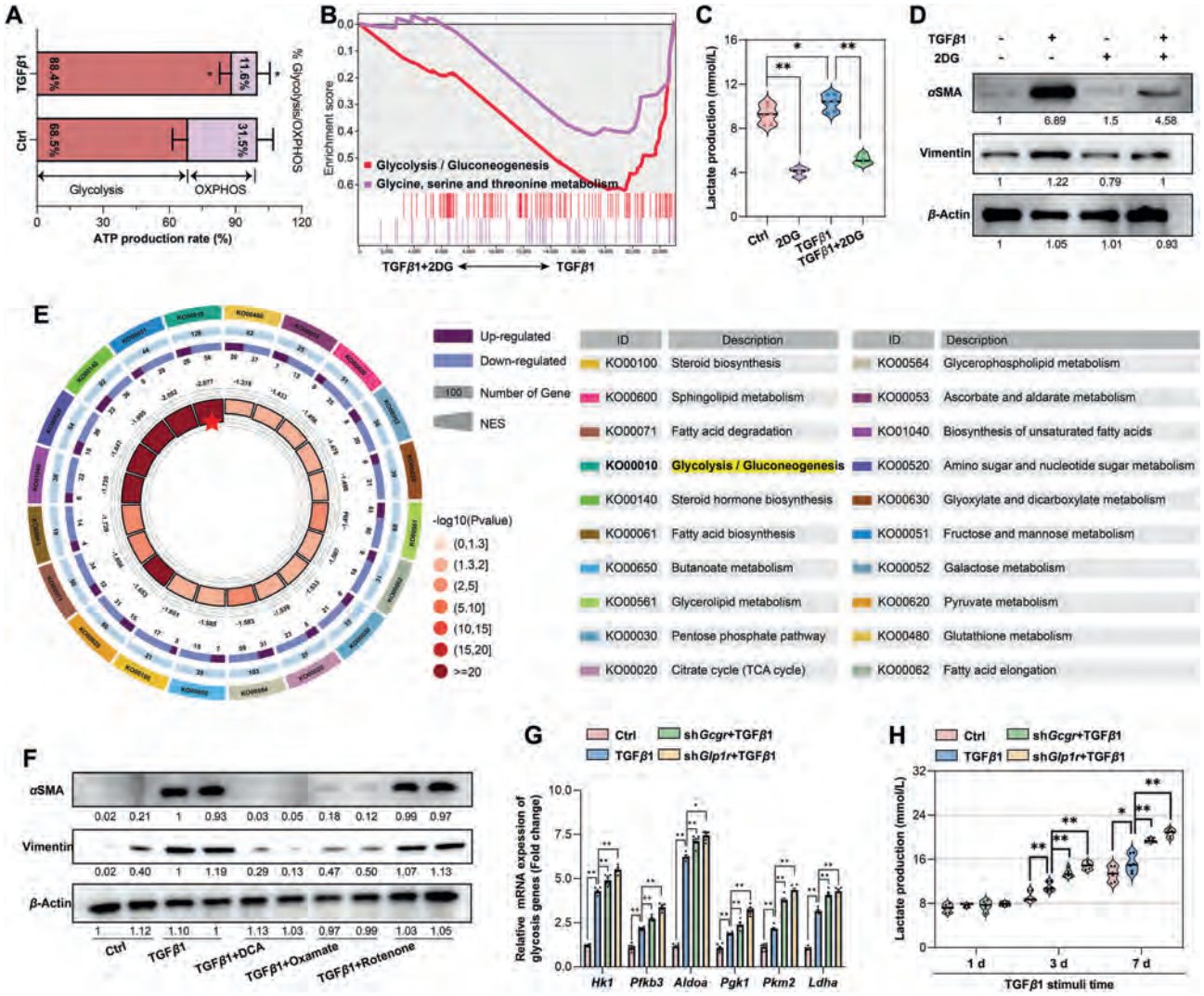

Figure 3 Lactate as glycolysis product promotes EMT in intestinal epithelial cells. (A) The relative ATP production rate was calculated in IEC6 cells stimulated or not with TGFβ1 (10 ng/mL) for 7 days ($n = 12$). The proportion of oxidative phosphorylation and glycolysis adds up to 100%. (B) GSEA-KEGG gene set enrichment analysis of microarray gene expression data ($n = 7-8$). (C) The influence of the glycolysis inhibitor 2DG (1 mmol/L) on TGFβ1-mediated extracellular lactate production ($n = 6$). The data are presented using violin plot. (D) The influence of 2DG on TGFβ1-mediated fibrosis-related protein expression ($n = 3$). (E) The enrichment plot of GSEA-KEGG shows the gene changes in metabolic-related datasets ($n = 7-8$). TGFβ1 *vs.* 2DG group. (F) The influence of oxamate (20 mmol/L), DCA (20 mmol/L), or rotenone (10 nmol/L) on Vimentin and αSMA protein expression ($n = 6$). (G) The effect of Lenti-*shGlp1r* or *Gcgr* on TGFβ1-mediated glycolysis-related genes ($n = 6$). (H) The effect of Lenti-*shGlp1r* or *Gcgr* on extracellular lactate production in IEC6 cells stimulating with TGFβ1 for 1, 3, or 7 days ($n = 6$). The data are presented using violin plot. Unless otherwise specified, the data are presented as the mean ± SEM. $^*P < 0.05$, $^{**}P < 0.01$ *vs* as indicated.

Additionally, sodium dichloroacetate (DCA) and oxamate were employed as the previous study to inhibit lactate production by modulating pyruvate dehydrogenase and lactate dehydrogenase (LDH) activities, respectively[38,39]. These compounds yielded results similar to 2DG, with DCA and oxamate causing a more pronounced reduction in fibrotic genes and proteins (Fig. 3F and Fig. S4F), leading to an increased lactate production (Fig. S4E). In contrast, using rotenone, a mitochondrial respiratory chain complex I inhibitor that drives glycolysis, increased the expression of fibrotic genes (Fig. S4F). Similar effects on fibrotic gene expression were observed in human adenocarcinoma colorectal cancer cell line SW480 (Fig. S4G). Therefore, it was concluded that downregulation of glycolysis and its product lactate improved intestinal EMT, while elevated lactate levels exacerbated the EMT process *in vitro*.

Lenti-sh*Glp1r* or *Gcgr*-infected epithelial cells were used to knockdown *Glp1r* or *Gcgr* (Supporting Information Fig. S5). Within the resulting stable knockdown cells, a further upregulation of the glycolytic genes and lactate level were triggered by TGFβ1 (Fig. 3G and H), indicating that lactate production was further improved by *Gcgr* or *Glp1r* knockdown *in vitro*. Overall, these findings demonstrated that the downregulation of GCGR and GLP1R led to lactate accumulation, thereby exacerbating intestinal fibrosis.

3.4. Lactate induced EMT-associated transcription though the regulation of H3K9 lactylation

Lactylation, a novel epigenetic modification occurring at the lysine residues of histones, is associated with transcriptional activation[40]. Given that lactate promoted the expression of the profibrotic mediators in intestinal epithelial cells, it was hypothesized that this effect was achieved through lactate-induced histone lactylation at the promoter regions of these profibrotic genes. Indeed, an increase of Pan-lysine lactylation (Pan Kla) was first confirmed in whole cell lysates as well as acid-extracted histones following endogenous and exogenous lactate induction (Fig. 4A, B and D). A considerable increase in lysine lactylation was observed in histones despite the use of pan anti-lactyl-lysine antibodies (Fig. 4C). Accordingly, qRT-PCR analysis showed significantly elevated expression of fibrotic genes after lactate stimulation (Fig. 4E), confirming that lactate induced histone lactylation and promoted profibrotic mediators.

Finally, the lactylation sites on histones were verified using antibodies against diverse forms of histone lactylation. Exogenous lactate induced overwhelming lactylation modifications in H2BK16la, H3K9la, H3K18la, H4K5la and H4K12la (Fig. 4F). Meanwhile TGFβ1-induced endogenous lactate upregulation resulted in lactylation of H2BK16la, H3K9la and H4K5la (Fig. 4G). Subsequently, mutants H2B (K16R), H3 (K9R), and H4 (K5R) were generated to introduce site-specific mutations to block lactylation for comparison with wild type (H2B, H3, H4) (Fig. 4H). Remarkably, cells overexpressing H3.1 (K9R) exhibited lower levels of fibrotic genes and proteins after treatment with lactate compared with the H3.1 WT group (Fig. 4I and J). However, overexpression of H2B (K16R) or H4 (K5R) did not display significant differences compared to the wild types after treatment with lactate (Fig. 4I and J).

To identify candidate genes regulated by histone lactylation, ChIP analysis was then performed. qChIP analysis demonstrated elevated H3K9la levels on Vimentin and *Tgfβ* promoters in intestinal epithelial cells, hinting at the potential functional significance of histone lactylation in EMT (Fig. 4K). A key acetyltransferase, p300, has been reported in histone lactylation process[11]. However, we found that the H3K9 lactylation exhibits a partial dependence on p300 (data not shown), implying the possible involvement of other transferases in mediating lactylation.

Taken together, lactate promotes the expression of profibrotic genes through H3K9 lactylation at their promoters, shedding light on the role of lactylation in intestinal fibrosis (Fig. 4L).

3.5. Simultaneous activation of GCGR and GLP1R ameliorates intestinal fibrosis by inhibiting glycolysis-driven histone lactylation in vitro

Downregulation of GCGR and GLP1R seemed to induce metabolic reprogramming, while the glycolysis product lactate was shown to regulate profibrotic transcription. A range of GCGR/GLP1R dual-target ultralong-acting peptides were synthesized, and their agonistic activities were assessed in HEK293 cells that stably expressed either human GLP1R or GCGR, using a cAMP response element-driven luciferase reporter (Table S1). The antifibrotic effects of these peptides were evaluated in a cell model, and identified the optimal peptide which was named 1907B (Supporting Information Fig. S6A and S6B).

To assess the effects of 1907B, the lead GLP1R/GCGR dual agonist peptide, on epithelial cells, a fluorescent molecule called fluorescein (FITC) was first synthesized and then attached to 1907B to track the localization. The structure diagram was displayed by Chimera (Fig. 5A), and the addition of FITC did not affect the agonistic activity of 1907B towards targets (Fig. 5B). After 24 h of incubation, 1907B-FITC was observed in the cell membrane (Fig. 5E), consistent with the positioning of G-protein coupled receptors.

In TGFβ1-induced epithelial cells, exposure to 1907B significantly decreased the expression of profibrotic factors (Fig. 5C, D, G and H), while in Lenti-sh*Glp1r* or *Gcgr*-infected cells, the effect was absent (Fig. S6C), implying that the activation of GLP1R and GCGR effectively inhibited the TGFβ1-driven EMT process *in vitro*.

Given the enhanced pro-fibrotic metabolic reprogramming *in vitro*, the effects of 1907B on the expression of glycolytic genes were subsequently explored. 1907B counteracted the stimulatory effects of TGFβ1 on these genes (Fig. 5K and L). 1907B also reduced the expression of enzymes within the serine−glycine biosynthetic pathway (Fig. S6E). Interestingly, the expression of the rate-limiting gluconeogenic enzymes *Pepck*, *Fbp1* and *G6pc*, which was repressed during fibrotic activation and inhibited by TGFβ1, was restored after 1907B treatment (Fig. S6D). Comparable effects on fibrotic gene expression and metabolic reprogramming were observed in SW480 cells treated with 1907B (Fig. S6F and S6G).

To confirm the effects of 1907B on glycolysis, seahorse XF analysis was performed, revealing that 1907B normalized the ATP production rate of glycolysis (Fig. 5F and I). Moreover, as a profibrotic mediator and glycolysis metabolite, extracellular lactate was significantly reduced in 1907B-treated epithelial cells (Fig. 5J). Additionally, 1907B inhibited the lactylation levels of promoters related to fibrosis genes (Fig. 5N) and ameliorated the predominant H3K9la induced by rotenone (Fig. 5M). Further, in the TGFβ1-induced cell model, 1907B significantly upregulated E-cadherin and downregulated Vimentin, αSMA, and H3K9la protein levels. However, with increasing doses of rotenone (lactate production inducer), the effect of 1907B decreased until it was completely abolished. This indicates that the action of 1907B depends on lactate, and upon reaching elevated lactate levels beyond the capacity of 1907B, its effects are diminished (Fig. S6H). Taken together, *in vitro* targeting of GCGR and GLP1R with 1907B during TGFβ1-driven metabolic reprogramming and EMT has antifibrotic potential in intestinal fibrosis.

3.6. GCGR/GLP1R dual-target peptide 1907B inhibits intestinal fibrosis in vivo

The antifibrotic potential of 1907B was examined in DSS and TNBS-induced chronic experimental colitis. In the DSS-induced model, 1907B treatment was initiated after the presence of substantial fibrotic tissues following two cycles of "2% DSS-water" which was repeated for three weeks. Given that reversing an established fibrosis can be challenging, a group treated with a high dose of 1907B at 240 μg/kg every other day was included. Treatment with 1907B also significantly reduced fecal blood scores (Supporting Information Fig. S7A), diarrhoea score (Fig. S7A), increased colonic length (Fig. 6A and B) as well as inflammation damage (Fig. 6F and Fig. S7C). More importantly, Masson and immunohistochemical staining for collagen confirmed the role of 1907B in reversing fibrosis not only in DSS (Fig. 6C and F) but also TNBS-induced colitis-associated colonic fibrosis model (Fig. S7D and S7E). Notably, treatment with 1907B significantly attenuated fibrosis-related and glycolysis-related genes or protein

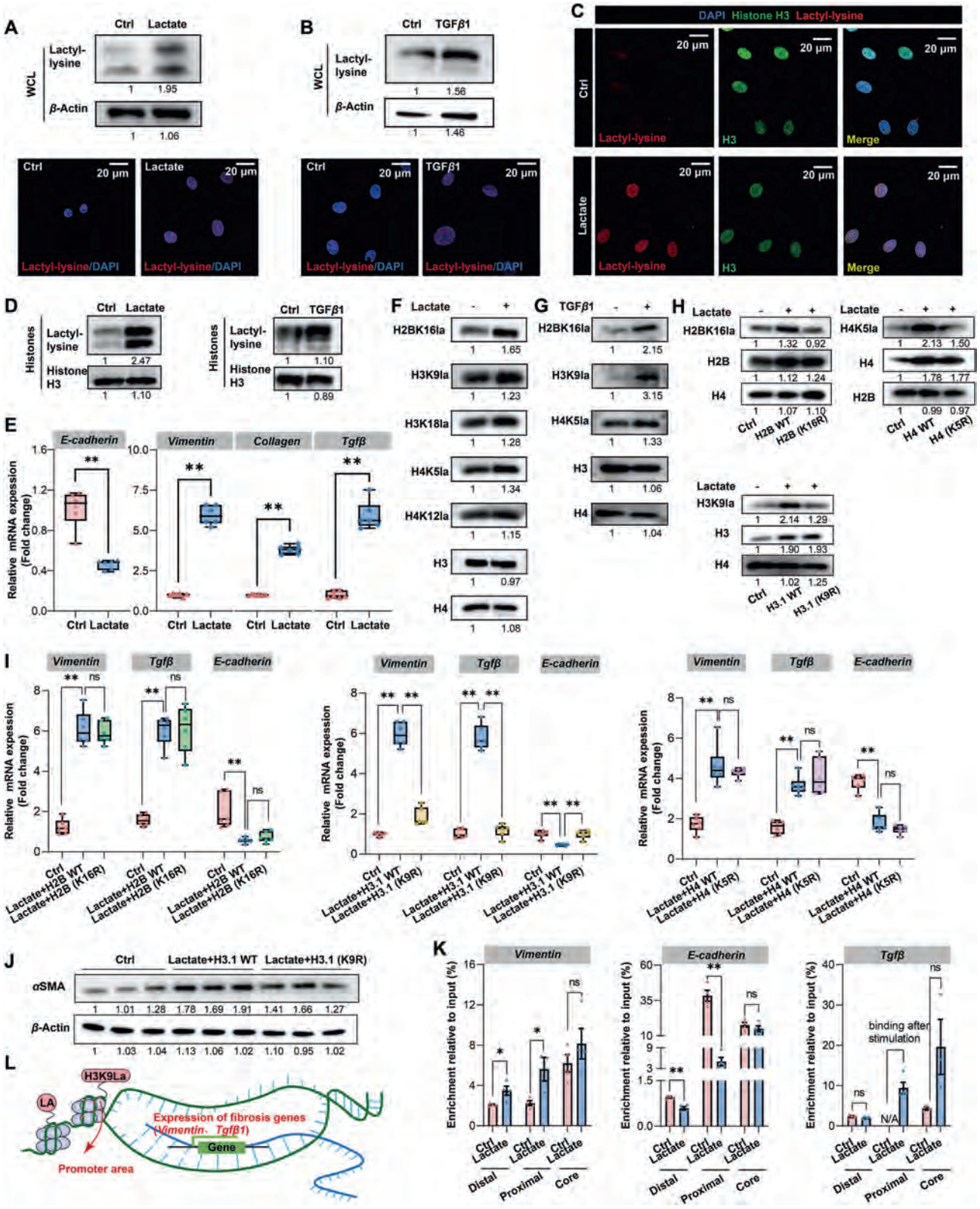

Figure 4 Lactate regulates EMT-related transcription through histone lactylation. (A, B) Representative Western blot images in whole cell lysates ($n = 3$) and immunofluorescent staining of lactyl-lysine ($n = 3$). IEC6 cells were treated with or without lactate (10 mmol/L) for 72 h, or treated with or without TGFβ1 (10 ng/mL) for 7 days. WCL = whole cell lysates. (C) Representative immunofluorescent staining is shown, demonstrating the co-localization of lactyl-lysine, histone 3 and DAPI ($n = 3$). (D) Representative Western blot images in HCl-extracted histones ($n = 3$). (E) The influence of lactate on fibrosis-related gene expression in IEC6 cells ($n = 6$). The data is presented as min to max using box plot. (F, G) Representative Western blot images of site-specific histone lactylation stimulated by lactate or TGFβ1 ($n = 3$). (H) Western blot images of

expression (Fig. 6D, E and K, Fig. S7B). GSEA analysis of the GO dataset confirmed the downregulation of genes related to fibrosis (Fig. 6H) and glycolysis (Fig. 6I) due to 1907B treatment, as evidenced by reduced gene expression in various categories. Additionally, the lactate level (Fig. 6J) and H3K9la expression (Fig. 6L) of intestine were ameliorated by 1907B. Immunofluorescence staining verified the upregulation of GCGR and GLP1R protein *in vivo* by 1907B (Fig. 6G). These findings further proved that co-activating GLP1R and GCGR can effectively inhibit intestinal fibrosis *in vivo* (Fig. 7).

4. Discussion

Accumulating evidence indicates the involvement of lactate in histone modifications within organ fibrosis, including lung and liver fibrosis[41-43]. This study introduces a novel perspective, highlighting dysregulated GCGR/GLP1R expression in intestinal fibrosis as a key driver of lactate accumulation and histone lactylation. This, in turn, promotes the process of EMT, a pivotal driver in fibrosis which is also implicated in the pathogenesis of various fibrotic diseases[44,45]. The groundbreaking peptide 1907B, designed to activate both GCGR and GLP1R, emerges as a promising candidate for mitigating intestinal fibrosis by effectively lowering lactate levels and H3K9 lactylation. Consequently, this research not only unveils fresh insights into the mechanisms underlying intestinal fibrosis but also underscores the potential of targeting the GCGR/GLP1R−lactate axis as a viable therapeutic approach.

In this study, the downregulation of GCGR and GLP1R in the fibrotic intestine of both human and mouse was confirmed before reporting the concomitant changes in energy metabolism. The reason for the downregulation of GCGR and GLP1R in intestinal fibrosis is complex. Apart from typical symptoms due to extensive intestinal inflammation, patients with IBD also suffer from malnutrition and metabolic disorders[46]. The downregulation of GCGR and GLP1R may be a response to altered nutrient availability, as these receptors are involved in regulating glycolipid and amino acid metabolism[47]. Regardless of the underlying reasons, the observed decrease in GCGR and GLP1R expression in intestinal fibrosis suggests a potential protective role for these receptors. The reduced expression of these proteins led to elevated levels of various metabolites, classified into OXPHOS, pentose phosphate pathway, glycolysis and TCA. Within these pathways, glycolysis was found to involve the maximum proportion of genes in intestinal fibrosis and the process was further increased after *Gcgr* and *Glp1r* knockdown. Among the several glycolytic byproducts, lactate content changed dramatically. The levels of glycerol-3-phosphate, 3-phosphoglycerate and pyruvic acid were also elevated, albeit to a lesser extent. While the focus of this study was on the GCGR/GLP1R−lactate axis, other metabolites such as pyruvic acid deserve further attention as intermediate metabolites of the TCA cycle, gluconeogenesis, fatty acid synthesis, acetone cycle and ketone body production[48-50].

TGFβ1 is a potent inducer of EMT, frequently employed to activate of EMT *in vitro*[51]. To assess fibrotic and reprogramming changes during EMT, three time points (1 day/3 days/7 days) were selected for observation. The findings revealed that *Gcgr* and *Glp1r* mRNA were downregulated following 3 days of TGFβ1 stimulation, accompanied by increased extracellular lactate production. These results were, in fact, consistent with previous observations in CD patients and DSS-induced mice. Lactate, a product of glycolysis and a substrate for mitochondrial respiration, is an essential metabolic link between glycolytic and aerobic pathways in mammalian systems[52]. To elucidate the causes of elevated lactate, OCR and ECAR were measured to compare the rates of glycolysis and aerobic pathways before evaluating the expression of glycolytic genes. The results suggested that glycolysis was the preferred energy source adopted by epithelial cells with fibroblast-like characteristics, as reflected in the higher expression of glycolytic genes and ECAR. The expression of glycolytic genes, including *Hk1*, *Pfkfb3*, *Aldoa*, *Pgk-1*, *Pkm2*, and *Ldha* in IEC6 cells, increased after 3 days and was further elevated after TGFβ1 stimulation for 7 days, resulting in lactate accumulation. Inhibiting glycolysis with 2DG significantly reduced extracellular lactate production, underscoring the substantial contribution of heightened glycolysis to lactate buildup.

Given that a decrease in GCGR and GLP1R was followed by elevated glycolysis and lactate production in the EMT cell model, co-activation these receptors could be a potential strategy to impede the process. Interestingly, a series of GCGR/GLP1R dual-target peptides were synthesized and evaluated in the cell model, with the optimal one named 1907B (>95% purity, Supporting Information Figs. S8 and S9). These series of peptides showed different activities towards GCGR and GLP1R, and an appropriate agonist ratio would be critical for their regulation of OXPHOS and glycolysis to induce their antifibrotic activity. For instance, it was noted that an agonist with an EC_{50} around 100 pmol/L for GLP1R and around 50 nmol/L for GCGR demonstrated enhanced therapeutic effects on intestinal fibrosis. However, the other dual-target peptides, named TB001 (EC_{50} of GLP1R = 0.04 nmol/L, EC_{50} of GCGR = 0.01 nmol/L, selectivity ratio of GCGR: GLP1R = 9.70), demonstrated therapeutic efficacy against hepatic fibrosis, but it did not show therapeutic effects in chronic colitis-associated intestinal fibrosis[23]. As mentioned by a highly insightful study, there remains uncertainty regarding the optimal activation of each receptor to achieve maximum benefit. We completely agree that a balance must be struck in the activation activity of GLP1R/GCGR dual agonists on both receptors, enhancing efficacy while mitigating corresponding toxic side effects. Starting from cryo-EM structures, Li et al.[53] elucidated the reasons for the different affinity of three peptides to the two targets. They identified key sequences, sites, and other factors influencing the peptide's activity on GLP1R/GCGR, with a focus on structure−activity relationship studies. What sets it apart is that we focused on the application of different activation ratios in fibrotic diseases, emphasizing the exploration from affinity to specific biological functions, thereby introducing novelty to our research. Hence, our study provides a novel contribution to the field of IBD and the application of GLP1R/GCGR.

In this study, 1907B could significantly increase GCGR and GLP1R protein and mRNA levels, thereby reducing expression of

site-specific histone lactylation protein in IEC6 cells after overexpression shRNAs transfection ($n = 3$). (I, J) The influence of histone site mutation on fibrosis-related gene ($n = 6$) or protein ($n = 3$) expression with lactate treatment. The data is presented as min to max using box plot. (K) Analysis of histone lactylation (H3K9la) levels by qChIP assay in the promoter regions of indicated genes in IEC6 cells treated with or without lactate ($n = 4$). The data is presented as the mean ± SEM. (L) A schematic diagram illustrates the relationship between histone lactylation and transcriptional regulation of EMT. $^*P < 0.05$, $^{**}P < 0.01$ *vs* as indicated. n.s. = not significant.

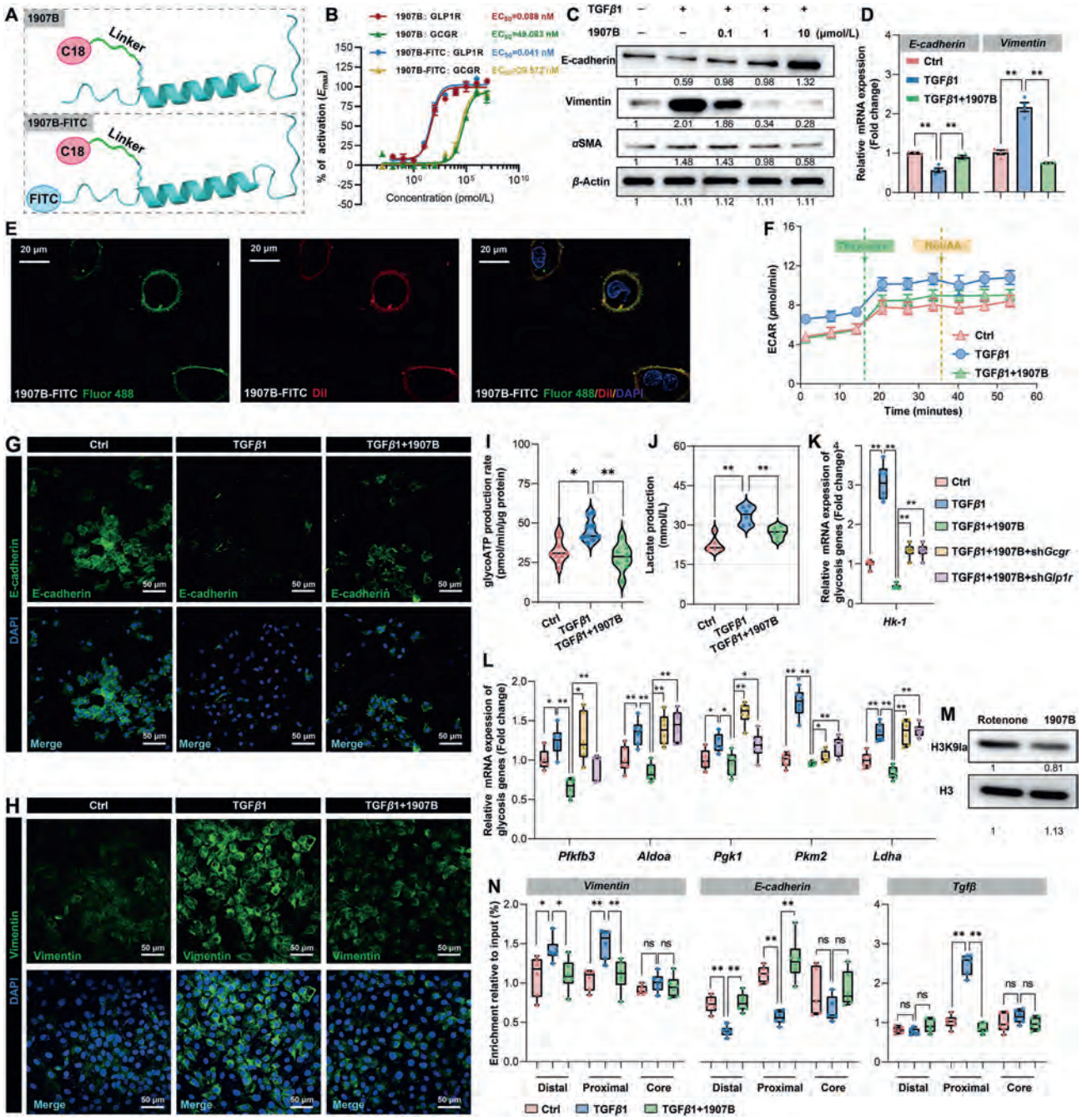

Figure 5 Dual activiating GCGR and GLP1R inhibits TGFβ1-driven metabolic reprogramming and EMT *in vitro*. (A) Design of dual agonist peptide 1907B and 1907B-FITC. C18 = C18 fatty acid, FITC = fluorescein. (B) GCGR/GLP1R-mediated cAMP synthesis by 1907B and 1907B-FITC ($n = 3$). (C) The influence of 1907B on TGFβ1-mediated fibrosis-related protein expression ($n = 3$). IEC6 cells were stimulated with TGFβ1 (10 ng/mL) and treated with 1907B for 7 days. (D) The influence of 1907B on E-cadherin and Vimentin gene expression in IEC6 cells ($n = 4$). The data is presented as the mean ± SEM. (E) Representative fluorescent images of the co-localization of 1907B-FITC and membrane in IEC6 cells after incubation with 1907B-FITC for 24 h ($n = 3$). (F) Extracellular acidification rate ($n = 9$). Data are presented as the mean ± SEM. (G, H) Representative immunofluorescent staining of E-cadherin and Vimentin ($n = 3$). (I) The influence of 1907B on the glycoATP production rate from glycolysis ($n = 9$). Data are presented using violin plot. (J) The influence of 1907B on TGFβ1-mediated lactate production ($n = 6$). Data are presented using violin plot. (K, L) The influence of 1907B on the glycolysis gene expression and the abolishing effect of Lenti-*shGlp1r* or *Gcgr* ($n = 6$). Data are presented as min to max using box plot. (M) Representative Western blot images of site-specific histone lactylation treated with 1907B ($n = 3$). (N) The influence of 1907B on histone lactylation (H3K9la) levels by qChIP assay ($n = 6$). Data are presented as min to max using box plot. $^*P < 0.05$, $^{**}P < 0.01$ *vs* as indicated. n.s. = not significant.

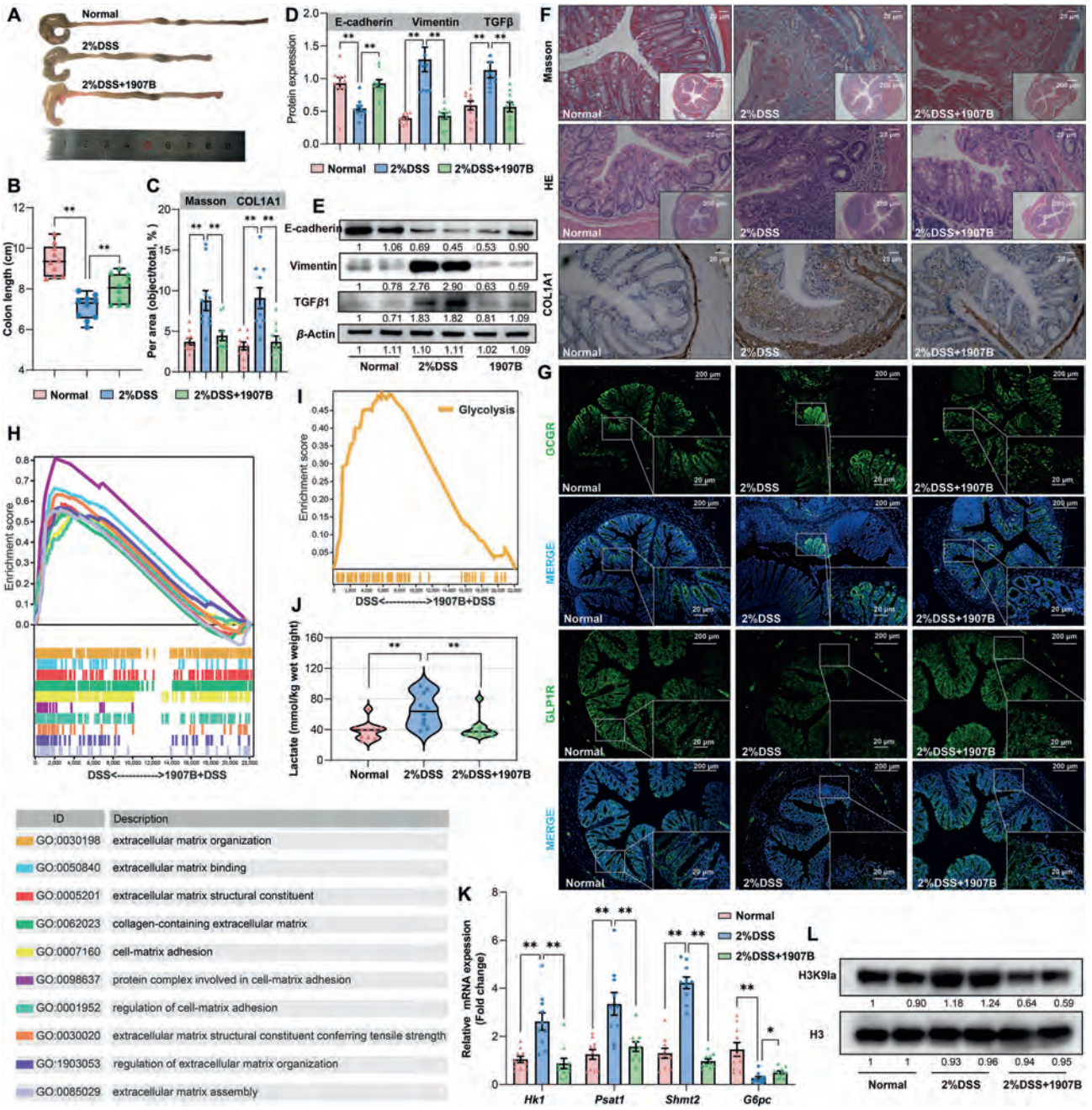

Figure 6 GCGR/GLP1R dual-target peptide 1907B inhibits intestinal fibrosis *in vivo*. (A, B) Gross morphology of the colon and colon length from the recipient mice ($n = 10$). (C) Semiquantitative image analyses of Masson staining ($n = 10$) and immunohistochemical staining for COL1A1 ($n = 10$). (D, E) Representative Western blot images and semiquantitative analysis of fibrosis protein are shown ($n = 10$). (F) Representative images of Masson staining, HE staining and immunohistochemical staining for COL1A1 ($n = 10$). (G) Representative immunofluorescent images of GCGR and GLP1R protein expression ($n = 10$). (H) GSEA-GO by RNA-sequencing reveals that extracellular-related genes are attenuated after 1907B treatment ($n = 3$ mice per group). (I) GSEA-Reactome by RNA-sequencing shows that glycolysis pathway genes are attenuated after 1907B treatment ($n = 3$ mice per group). (J) The influence of 1907B on lactate production in intestine ($n = 10$). Data are presented using violin plot. (K) The influence of 1907B on the glycolysis gene expression in intestine ($n = 10$). (L) Representative Western blot images of site-specific H3K9la ($n = 10$). Unless otherwise specified, Data are presented as the mean ± SEM. $^*P < 0.05$, $^{**}P < 0.01$ *vs* as indicated.

glycolytic enzymes and lactate. However, it remains unclear how the downstream molecule lactate, as a byproduct of glycolysis, affects intestinal fibrosis. In keloid skin fibroblasts, lactate production is higher by 50% compared with normal skin fibroblasts, linked with lactate dehydrogenase upregulation[54]. Similar increases in lactate production have been observed in a mouse model of renal interstitial fibrosis where transcription of hexokinase and pyruvate kinase was higher[55]. The current study confirms that lactate production promotes intestinal fibrosis, as evidenced by the downregulation of fibrotic genes with DCA or oxamate

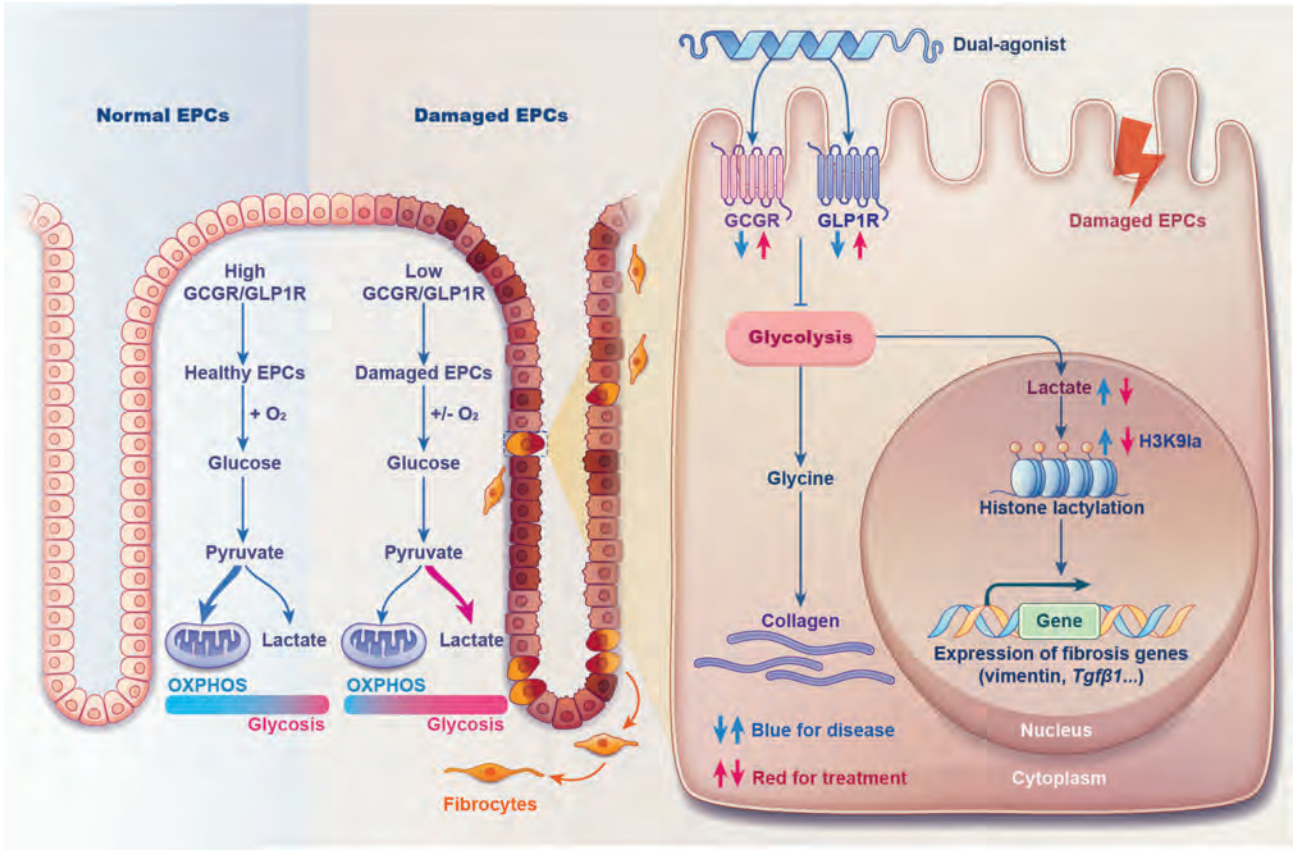

Figure 7 Schematic illustration of the research. GCGR/GLP1R—lactate axis regulates H3K9 lactylation to activate transcription of fibrosis genes in epithelial cells. Cotargeting GCGR/GLP1R shows potential in the treatment of intestinal fibrosis (EPC, epithelial cells).

(lactate production inhibitors[56,57]), as well as the upregulation of these genes with rotenone (lactate production inducer[58]). Recently, Zhang et al.[11] reported a novel function of glycolysis-derived lactate in macrophages where it is utilized to modify nuclear histones by adding lactyl groups to their lysine residues. This process may explain the profibrotic effect of lactate. Similarly, this study revealed that lactate could induce H3K9 lactylation in the promoter regions of Vimentin and *Tgfβ1*, while decreasing lactylation of E-cadherin. These results suggested that H3K9 lactylation can directly promote or inhibit gene transcription under the above conditions. Indeed, this study demonstrated that epithelial cells with fibroblast characteristics exhibit upregulated Vimentin and *Tgfβ1* expression through epigenetic mechanisms involving increased promoter region lactylation, which was countered by 1907B. The current findings align with prior studies that have highlighted the significance of epigenetic changes in regulating the expression of fibrotic genes. Although the function of lactate and histone lactylation in fibrosis is yet to be fully explored, this work offers novel evidence supporting their contribution in this mechanism.

It was observed that using 1907B to pharmacologically target GCGR and GLP1R successfully mitigated the pro-fibrotic responses and metabolic reprogramming associated with DSS-induced mouse chronic colitis. This promising outcome indicating that targeting these receptors could be an effective treatment for intestinal fibrosis. Additionally, the safety of 1907B in humans is currently being verified *via* a phase I clinical trial (approved No. 2022LP01773). However, additional research is required to determine the effectiveness of this peptide in humans and to establish the optimal dosage and treatment plan.

In this study, lactate accumulation and histone H3K9 lactylation were considered the detrimental factor in colitis-associated colonic fibrosis, while Wang et al.[59] suggested that dietary lactate supplementation alleviated acute colitis in an acute colitis model of pig. Indeed, the tissue microenvironment of acute colitis differs from that of chronic colitis, in terms of both inflammatory and metabolic environments. Lactate may exert varying effects depending on tissue microenvironment, cell type, and metabolic status. For example, lactate exhibits both pro-inflammatory and anti-inflammatory effects: Comito et al.[60] suggested that lactate promoted the generation and function of regulatory T cells, exerting anti-inflammatory effects; while Quiroga et al.[61] observed that lactate induced pro-inflammatory genes and metabolic genes in a phosphatidylinositol 3-kinase/protein kinase B-dependent manner, as well as in a HIF-1/NF-κB-dependent manner. Additionally, in chronic diseases, Fan et al.[62] indicated that lactate promoted hypoxia-induced endothelial-to-mesenchymal transition and activate the TGF-β/Smad2 signaling pathway, leading to increased cardiac fibrosis, while did not affect the phosphorylation of Smad3 following normoxic or hypoxic challenge. In our observation, lactate treatment did not alter the phosphorylation of either Smad2 or Smad3. Therefore, the role of lactate in diseases is complex, and further research is needed to address this issue. We will continue to query and follow the literature in this area to address this question in the future.

Previous studies have shown that GCGR and GLP1R can impede fibrosis in the liver[22]. However, this study stands out as the

first one to uncover the crucial role of the GCGR/GLP1R−lactate axis in intestinal fibrosis, and to identify histone lactylation as a mechanism underlying lactate-induced profibrotic gene expression. Lactylation modification was recently discovered in macrophages, so the research on lactylation in the perspective of epithelial cells, as a type of stromal cell, is highly novel. These findings have several implications for the diagnosis and treatment of intestinal fibrosis. First, it highlights the significance of the GCGR/GLP1R−lactate axis in the pathogenesis of this disease, suggesting that targeting these receptors could be an effective therapeutic strategy. Secondly, it identifies histone lactylation as a potential target for intervention in fibrosis. Finally, this research provides fresh insights into the mechanisms of EMT and fibrosis, highlighting lactate as a potential biomarker for fibrotic disorders. Of course, limitations exist, such as the gene knockout mice with intestinal epithelial cell specificity, which implies better specificity than AAV9 but entails higher costs and potential risks of mouse mortality.

5. Conclusions

This study uncovers, for the first time, the GCGR/GLP1R−lactate axis as a feasible and promising mechanism for intestinal fibrosis, in which the regulation of H3K9 lactylation activates transcription of fibrosis genes. Simultaneously activating GCGR/GLP1R therefore might have great potential in treating patients with intestinal fibrosis.

Acknowledgments

This work was supported by the National Key R&D Program of China (2023YFC2507300), the National Natural Science Foundation of China (82273761, 81970483, 82170537 and 82222010) and the Medical Innovation and Development Project of Lanzhou University (lzuyxcx-2022-156, China).

Author contributions

Han Liu: Writing − review & editing, Writing − original draft, Validation, Resources, Project administration, Methodology, Investigation, Formal analysis, Data curation, Conceptualization. Yujie Hong: Methodology, Formal analysis, Data curation. Hui Chen: Methodology, Investigation. Xianggui Wang: Visualization, Validation, Methodology, Formal analysis, Data curation. Jiale Dong: Writing − review & editing, Visualization, Validation, Methodology, Investigation, Conceptualization. Xiaoqian Li: Visualization, Methodology, Formal analysis, Data curation. Zihan Shi: Methodology. Qian Zhao: Resources, Investigation. Longyuan Zhou: Writing − review & editing, Validation, Software, Methodology. JiaXin Wang: Software, Methodology, Investigation. Qiuling Zeng: Methodology. Qinglin Tang: Methodology. Qi Liu: Resources. Florian Rieder: Writing − review & editing, Validation, Investigation. Baili Chen: Resources, Investigation. Minhu Chen: Supervision, Investigation, Funding acquisition. Rui Wang: Writing − review & editing, Supervision, Resources, Investigation, Funding acquisition. Yao Zhang: Writing − review & editing, Validation, Software, Formal analysis. Ren Mao: Writing − review & editing, Supervision, Resources, Investigation, Funding acquisition. Xianxing Jiang: Writing − review & editing, Supervision, Resources, Project administration, Investigation, Funding acquisition.

Conflicts of interest

Florian Rieder was consultant to Adnovate, Agomab, Allergan, AbbVie, Arena, Boehringer-Ingelheim, Celgene/BMS, CDISC, Celsius, Cowen, Ferring, Galapagos, Galmed, Genentech, Gilead, Gossamer, Granite, Guidepoint, Helmsley, Horizon Therapeutics, Image Analysis Limited, Index Pharma, Landos, Jannsen, Koutif, Mestag, Metacrine, Mopac, Morphic, Organovo, Origo, Pfizer, Pliant, Prometheus Biosciences, Receptos, RedX, Roche, Samsung, Sanofi, Surmodics, Surrozen, Takeda, Techlab, Teva, Theravance, Thetis, UCB, Ysios, 89Bio.

Appendix A. Supporting information

Supporting information to this article can be found online at https://doi.org/10.1016/j.apsb.2024.11.017.

References

1. Lin SN, Mao R, Qian C, Bettenworth D, Wang J, Li J, et al. Development of antifibrotic therapy for stricturing Crohn's disease: lessons from randomized trials in other fibrotic diseases. *Physiol Rev* 2022;**102**:605−52.
2. Santacroce G, Lenti MV, Di Sabatino A. Therapeutic targeting of intestinal fibrosis in Crohn's disease. *Cells* 2022;**11**:429.
3. Monteleone G, Boirivant M, Pallone F, MacDonald TT. TGF-beta1 and Smad7 in the regulation of IBD. *Mucosal Immunol* 2008;**1**(Suppl 1):S50−3.
4. Lovisa S, Genovese G, Danese S. Role of epithelial-to-mesenchymal transition in inflammatory bowel disease. *J Crohns Colitis* 2019;**13**: 659−68.
5. Liu P, Gao C, Chen H, Vong CT, Wu X, Tang X, et al. Receptor-mediated targeted drug delivery systems for treatment of inflammatory bowel disease: opportunities and emerging strategies. *Acta Pharm Sin B* 2021;**11**:2798−818.
6. Henderson J, O'Reilly S. The emerging role of metabolism in fibrosis. *Trends Endocrinol Metab* 2021;**32**:639−53.
7. Cui H, Xie N, Banerjee S, Ge J, Jiang D, Dey T, et al. Lung myofibroblasts promote macrophage profibrotic activity through lactate-induced histone lactylation. *Am J Respir Cell Mol Biol* 2021;**64**:115−25.
8. Liu W, Wang Y, Bozi LHM, Fischer PD, Jedrychowski MP, Xiao H, et al. Lactate regulates cell cycle by remodelling the anaphase promoting complex. *Nature* 2023;**616**:790−7.
9. Gu J, Zhou J, Chen Q, Xu X, Gao J, Li X, et al. Tumor metabolite lactate promotes tumorigenesis by modulating MOESIN lactylation and enhancing TGF-beta signaling in regulatory T cells. *Cell Rep* 2022;**39**:110986.
10. Wang J, Yang P, Yu T, Gao M, Liu D, Zhang J, et al. Lactylation of PKM2 suppresses inflammatory metabolic adaptation in pro-inflammatory macrophages. *Int J Biol Sci* 2022;**18**:6210−25.
11. Zhang D, Tang Z, Huang H, Zhou G, Cui C, Weng Y, et al. Metabolic regulation of gene expression by histone lactylation. *Nature* 2019;**574**: 575−80.
12. Yang Z, Yan C, Ma J, Peng P, Ren X, Cai S, et al. Lactylome analysis suggests lactylation-dependent mechanisms of metabolic adaptation in hepatocellular carcinoma. *Nat Metab* 2023;**5**:61−79.
13. Xiong J, He J, Zhu J, Pan J, Liao W, Ye H, et al. Lactylation-driven METTL3-mediated RNA m^6A modification promotes immunosuppression of tumor-infiltrating myeloid cells. *Mol Cell* 2022;**82**: 1660−77. e10.
14. Wan N, Wang N, Yu S, Zhang H, Tang S, Wang D, et al. Cyclic immonium ion of lactyllysine reveals widespread lactylation in the human proteome. *Nat Methods* 2022;**19**:854−64.
15. Dong M, Zhang Y, Chen M, Tan Y, Min J, He X, et al. ASF1A-dependent P300-mediated histone H3 lysine 18 lactylation promotes atherosclerosis by regulating EndMT. *Acta Pharm Sin B* 2024;**14**: 3027−48.

16. Jiang J, Huang D, Jiang Y, Hou J, Tian M, Li J, et al. Lactate modulates cellular metabolism through histone lactylation-mediated gene expression in non-small cell lung cancer. *Front Oncol* 2021;**11**:647559.
17. Hailiwu R, Zeng H, Zhan M, Pan T, Yang H, Li P. Salvianolic acid A diminishes LDHA-driven aerobic glycolysis to restrain myofibroblasts activation and cardiac fibrosis *via* blocking Akt/GSK-3beta/HIF-1alpha axis. *Phytother Res* 2023;**37**:4540−56.
18. Rho H, Terry AR, Chronis C, Hay N. Hexokinase 2-mediated gene expression *via* histone lactylation is required for hepatic stellate cell activation and liver fibrosis. *Cell Metab* 2023;**35**:1406−23. e8.
19. Yang Q, Huo E, Cai Y, Zhang Z, Dong C, Asara JM, et al. PFKFB3-mediated glycolysis boosts fibroblast activation and subsequent kidney fibrosis. *Cells* 2023;**12**:2081.
20. Malavazos AE, Iacobellis G, Dozio E, Basilico S, Di Vincenzo A, Dubini C, et al. Human epicardial adipose tissue expresses glucose-dependent insulinotropic polypeptide, glucagon, and glucagon-like peptide-1 receptors as potential targets of pleiotropic therapies. *Eur J Prev Cardiol* 2023;**30**:680−93.
21. Shao L, Chen Y, Zhang S, Zhang Z, Cao Y, Yang D, et al. Modulating effects of RAMPs on signaling profiles of the glucagon receptor family. *Acta Pharm Sin B* 2022;**12**:637−50.
22. Boland ML, Laker RC, Mather K, Nawrocki A, Oldham S, Boland BB, et al. Resolution of NASH and hepatic fibrosis by the GLP-1R/GcgR dual-agonist Cotadutide *via* modulating mitochondrial function and lipogenesis. *Nat Metab* 2020;**2**:413−31.
23. Song N, Xu H, Liu J, Zhao Q, Chen H, Yan Z, et al. Design of a highly potent GLP-1R and GCGR dual-agonist for recovering hepatic fibrosis. *Acta Pharm Sin B* 2022;**12**:2443−61.
24. Jouihan H, Will S, Guionaud S, Boland ML, Oldham S, Ravn P, et al. Superior reductions in hepatic steatosis and fibrosis with co-administration of a glucagon-like peptide-1 receptor agonist and obeticholic acid in mice. *Mol Metab* 2017;**6**:1360−70.
25. Bang-Berthelsen CH, Holm TL, Pyke C, Simonsen L, Sokilde R, Pociot F, et al. GLP-1 induces barrier protective expression in Brunner's glands and regulates colonic inflammation. *Inflamm Bowel Dis* 2016;**22**:2078−97.
26. Yusta B, Baggio LL, Koehler J, Holland D, Cao X, Pinnell LJ, et al. GLP-1R agonists modulate enteric immune responses through the intestinal intraepithelial lymphocyte GLP-1R. *Diabetes* 2015;**64**: 2537−49.
27. Koehler JA, Baggio LL, Yusta B, Longuet C, Rowland KJ, Cao X, et al. GLP-1R agonists promote normal and neoplastic intestinal growth through mechanisms requiring Fgf7. *Cell Metab* 2015;**21**: 379−91.
28. Mao R, Doyon G, Gordon IO, Li J, Lin S, Wang J, et al. Activated intestinal muscle cells promote preadipocyte migration: a novel mechanism for creeping fat formation in Crohn's disease. *Gut* 2022; **71**:55−67.
29. Wirtz S, Neufert C, Weigmann B, Neurath MF. Chemically induced mouse models of intestinal inflammation. *Nat Protoc* 2007;**2**:541−6.
30. Fang Y, Shen ZY, Zhan YZ, Feng XC, Chen KL, Li YS, et al. CD36 inhibits beta-catenin/c-myc-mediated glycolysis through ubiquitination of GPC4 to repress colorectal tumorigenesis. *Nat Commun* 2019; **10**:3981.
31. Ren HJ, Cui J, Wang ZQ, Liu RD. Normal mouse intestinal epithelial cells as a model for the *in vitro* invasion of Trichinella spiralis infective larvae. *PLoS One* 2011;**6**:e27010.
32. Liu H, Wang Y, Han Y, Yang G, Wang L, Peng J, et al. Pretreatment optimization of tissue metabolomics in colorectal cancer. *Asia Pac J Clin Nutr* 2022;**31**:526−33.
33. Brown DG, Rao S, Weir TL, O'Malia J, Bazan M, Brown RJ, et al. Metabolomics and metabolic pathway networks from human colorectal cancers, adjacent mucosa, and stool. *Cancer Metab* 2016;**4**:11.
34. Rodriguez-Collazo P, Leuba SH, Zlatanova J. Robust methods for purification of histones from cultured mammalian cells with the preservation of their native modifications. *Nucleic Acids Res* 2009;**37**:e81.
35. Hasbrouck NC, High KA. AAV-mediated gene transfer for the treatment of hemophilia B: problems and prospects. *Gene Ther* 2008;**15**:870−5.
36. Zhao Q, Dong J, Liu H, Chen H, Yu H, Ye S, et al. Design and discovery of a highly potent ultralong-acting GLP-1 and glucagon co-agonist for attenuating renal fibrosis. *Acta Pharm Sin B* 2024;**14**: 1283−301.
37. Polyak S, Mach A, Porvasnik S, Dixon L, Conlon T, Erger KE, et al. Identification of adeno-associated viral vectors suitable for intestinal gene delivery and modulation of experimental colitis. *Am J Physiol Gastrointest Liver Physiol* 2012;**302**:G296−308.
38. Tso SC, Qi X, Gui WJ, Wu CY, Chuang JL, Wernstedt-Asterholm I, et al. Structure-guided development of specific pyruvate dehydrogenase kinase inhibitors targeting the ATP-binding pocket. *J Biol Chem* 2014;**289**:4432−43.
39. Muramatsu H, Sumitomo M, Morinaga S, Kajikawa K, Kobayashi I, Nishikawa G, et al. Targeting lactate dehydrogenase-A promotes docetaxel-induced cytotoxicity predominantly in castration-resistant prostate cancer cells. *Oncol Rep* 2019;**42**:224−30.
40. Wang X, Fan W, Li N, Ma Y, Yao M, Wang G, et al. YY1 lactylation in microglia promotes angiogenesis through transcription activation-mediated upregulation of FGF2. *Genome Biol* 2023;**24**:87.
41. Hagood JS. Beyond the genome: epigenetic mechanisms in lung remodeling. *Physiology* 2014;**29**:177−85.
42. Xue T, Qiu X, Liu H, Gan C, Tan Z, Xie Y, et al. Epigenetic regulation in fibrosis progress. *Pharmacol Res* 2021;**173**:105910.
43. Moran-Salvador E, Mann J. Epigenetics and liver fibrosis. *Cell Mol Gastroenterol Hepatol* 2017;**4**:125−34.
44. Nieto MA, Huang RY, Jackson RA, Thiery JP. Emt: 2016. *Cell* 2016; **166**:21−45.
45. Grande MT, Sanchez-Laorden B, Lopez-Blau C, De Frutos CA, Boutet A, Arevalo M, et al. Snail1-induced partial epithelial-to-mesenchymal transition drives renal fibrosis in mice and can be targeted to reverse established disease. *Nat Med* 2015;**21**:989−97.
46. Zatorski H, Salaga M, Fichna J. Role of glucagon-like peptides in inflammatory bowel diseases-current knowledge and future perspectives. *Naunyn Schmiedebergs Arch Pharmacol* 2019;**392**:1321−30.
47. Zietek T, Waldschmitt N, Rath E. Role of incretin hormones in bowel diseases. *Endocr Dev* 2017;**32**:49−73.
48. Ricci L, Stanley FU, Eberhart T, Mainini F, Sumpton D, Cardaci S. Pyruvate transamination and NAD biosynthesis enable proliferation of succinate dehydrogenase-deficient cells by supporting aerobic glycolysis. *Cell Death Dis* 2023;**14**:403.
49. Lee WD, Liang L, AbuSalim J, Jankowski CSR, Samarah LZ, Neinast MD, et al. Impact of acute stress on murine metabolomics and metabolic flux. *Proc Natl Acad Sci U S A* 2023;**120**:e2301215120.
50. Ni J, Zhang H, Wang X, Liu Z, Nie T, Li L, et al. Rg3 regulates myocardial pyruvate metabolism *via* P300-mediated dihydrolipoamide dehydrogenase 2-hydroxyisobutyrylation in TAC-induced cardiac hypertrophy. *Cell Death Dis* 2022;**13**:1073.
51. Kasai H, Allen JT, Mason RM, Kamimura T, Zhang Z. TGF-beta1 induces human alveolar epithelial to mesenchymal cell transition (EMT). *Respir Res* 2005;**6**:56.
52. Vander Heiden MG, Cantley LC, Thompson CB. Understanding the Warburg effect: the metabolic requirements of cell proliferation. *Science* 2009;**324**:1029−33.
53. Li Y, Zhou QT, Dai AT, Zhao FH, Chang RL, Ying TL, et al. Structural analysis of the dual agonism at GLP-1R and GCGR. *P Natl Acad Sci USA* 2023;**120**:e2303696120.
54. Vincent AS, Phan TT, Mukhopadhyay A, Lim HY, Halliwell B, Wong KP. Human skin keloid fibroblasts display bioenergetics of cancer cells. *J Invest Dermatol* 2008;**128**:702−9.
55. Yin XN, Wang J, Cui LF, Fan WX. Enhanced glycolysis in the process of renal fibrosis aggravated the development of chronic kidney disease. *Eur Rev Med Pharmacol Sci* 2018;**22**:4243−51.
56. Xiang J, Zhou L, He Y, Wu S. LDH-A inhibitors as remedies to enhance the anticancer effects of PARP inhibitors in ovarian cancer cells. *Aging (Albany NY)* 2021;**13**:25920−30.
57. Sun L, Xiong H, Chen L, Dai X, Yan X, Wu Y, et al. Deacetylation of ATG4B promotes autophagy initiation under starvation. *Sci Adv* 2022;**8**: eabo0412.

58. Lien EC, Westermark AM, Zhang Y, Yuan C, Li Z, Lau AN, et al. Low glycaemic diets alter lipid metabolism to influence tumour growth. *Nature* 2021;**599**:302−7.
59. Wang M, Fan Z, Chen D, Yu B, He J, Yu J, et al. Dietary lactate supplementation can alleviate DSS-induced colitis in piglets. *Biomed Pharmacother* 2023;**158**:114148.
60. Comito G, Iscaro A, Bacci M, Morandi A, Ippolito L, Parri M, et al. Lactate modulates $CD4^+$ T-cell polarization and induces an immunosuppressive environment, which sustains prostate carcinoma progression *via* TLR8/miR21 axis. *Oncogene* 2019;**38**: 3681−95.
61. Quiroga J, Alarcon P, Manosalva C, Teuber S, Taubert A, Hermosilla C, et al. Metabolic reprogramming and inflammatory response induced by D-lactate in bovine fibroblast-like synoviocytes depends on HIF-1 activity. *Front Vet Sci* 2021;**8**:625347.
62. Fan M, Yang K, Wang X, Chen L, Gill PS, Ha T, et al. Lactate promotes endothelial-to-mesenchymal transition *via* Snail1 lactylation after myocardial infarction. *Sci Adv* 2023;**9**:eadc9465.